Numerical Study on the Buckling Behavior of Austenitic Stainless Steel Unequal-Leg Angle Columns

EDWARD J. SIPPEL and HANNAH B. BLUM

ABSTRACT

A computational-based parametric study on stainless steel unequal-leg angles with various end conditions was conducted to assess the buckling behavior and comparison to ANSI/AISC 370 provisions. Experimental work completed at the University of Wisconsin–Madison subjected hot-rolled Grade 304 austenitic stainless steel unequal-leg angles, ranging in length from 10 to 148 in., to uniform compression with fixed supports. The angles failed in flexural-torsional buckling with variable degrees of flexural and torsional deformations. This paper reports on the finite element modeling validation of the flexural-torsional buckling failures and subsequent 2,880-model parametric study. The finite element analysis utilized a simplified approach that isolated the angle column with perfect fixed-fixed boundary conditions and incorporated measured material properties, cross-section dimensions, and geometric imperfections. This method accurately simulated the appropriate nonlinear stiffness, deflection patterns, and ultimate capacities associated with the torsion-dominated buckling failures. Flexure-dominated failures of the long specimens were not as accurately predicted by this modeling; however, the assumption of continuous positive contact and a perfect bearing surface was noted to be inaccurate. Further investigation noted that accounting for imperfect bearing and plastic deformation of the base plates from previous tests captured the reduced ultimate capacity and ductility of the column, similar to what was observed in testing. Therefore, the base modeling technique was adequate to conduct a parametric study that utilizes perfect supports. The evaluation of 12 nonslender-element unequal-leg angles, considering both nominal and measured material properties supported by fixed-fixed or pinned-pinned boundary conditions, provided additional data to qualify the behavior of unequal-leg single angles. Considering the nominal stress-strain response indicated in AISC 370, flexural-torsional buckling is consistently observed as the overall failure mode with transitions from flexural buckling dominated to torsional buckling dominated behavior. Comparisons to existing AISC 370 strength provisions indicated that the direct consideration of flexural-torsional buckling was necessary to conservatively predict the capacity. However, accounting for the measured stress-strain response resulted in a substantially higher tangent stiffness before yielding compared to the nominal response, which led to a change in overall behavior. Similar flexural-torsional buckling failures were observed, but the increased stiffness reduced the impact from the onset of increased torsional buckling participation at maximum load. The reduced design capacity from considering flexural-torsional buckling was not needed to obtain a conservative result. Instead, the flexural buckling provisions alone resulted in reasonable predictions of strength for the nonslender-element cross sections. This result is not enough evidence to change ANSI/AISC 370 provisions; however, it highlights the importance in confirming the nominal stress-strain behavior of hot-rolled stainless steel angles for compression design as this assumption could alter the importance of considering flexural-torsional buckling.

Keywords: stainless steel, unequal-leg angles, flexural-torsional buckling, flexural buckling, compression member.

INTRODUCTION

The recent release of the AISC *Specification for Structural Stainless Steel Buildings*, ANSI/AISC 370, (2021), hereafter referred to as AISC 370, has provided additional opportunities to implement stainless steel members and take advantage of their corrosion resistance, thermal properties, and aesthetics among other benefits (Houska, 2014).

Edward J. Sippel, Assistant Professor, Milwaukee School of Engineering, Milwaukee, Wis. Formerly, Graduate Research Assistant, University of Wisconsin–Madison. Email: sippel@msoe.edu (corresponding)

Hannah B. Blum, Alain H. Peyrot Associate Professor, University of Wisconsin–Madison, Madison, Wis. Email: hannah.blum@wisc.edu

Paper No. 2023-10R

AISC 370 provides an approved design procedure to evaluate members in compression, including nonslender-element, equal-leg single angles. Unlike carbon steel members designed according to the AISC *Specification for Structural Steel Buildings*, ANSI/AISC 360 (2022), hereafter referred to as AISC 360, the stainless steel provisions incorporate a three-stage buckling model that separates the response into full member yield, inelastic buckling, and elastic buckling. Another difference introduced to the stainless steel design procedure is the consideration of flexural-torsional buckling with single angles. This is a change from guidance provided in the first edition AISC Design Guide 27, *Structural Stainless Steel* (Baddoo, 2013), which aligned with the design provisions for carbon steel single angles that permitted excluding the direct calculation of flexural-torsional buckling because the local buckling reduction adequately reduces the flexural buckling capacity to produce a safe

design (Galambos, 1991). There is interest in expanding the available data for unequal-leg angles subjected to uniform compression such that the new provisions can be properly assessed with regard to the capacity and the types of failure modes checked.

Material Properties

Stainless steel exhibits a nonlinear stress-strain response, as shown in Figure 1, unlike typical structural carbon steels. While carbon steels have a well-defined yield behavior, stainless steels have no definitive yield point. Stainless steel behavior is characterized by a departure from the linear elastic response at low stresses, which varies with the exact material alloy. The yield point is alternatively defined using a specified offset strain, commonly 0.2% strain as highlighted in Figure 1.

Various models (Dundu, 2018) have been considered to capture the nonlinear behavior of stainless steel, with the most popular ones being based on the modified Ramberg-Osgood model (Hill, 1944). While this model has been shown to effectively capture stresses below the yield stress, it regularly overpredicts observed stresses at higher strains as shown in Figure 2. Researchers have addressed this issue in different ways (MacDonald et al., 2000; Olsson, 2001; Mirambell and Real, 2000; Rasmussen, 2003; Gardner and Nethercot, 2004; Gardner and Ashraf, 2006; Quach et al., 2008; Hradil et al., 2013); however, one of the more common solutions is the application of a two-stage, modified Ramberg-Osgood stress-strain relationship as shown in Equation 1:

$$\varepsilon = \begin{cases} \dfrac{f}{E_0} + 0.002\left(\dfrac{f}{f_{0.2}}\right)^n & \text{if } f \le f_{0.2} \\ \dfrac{f - f_{0.2}}{E_{0.2}} + \varepsilon_{max}\left(\dfrac{f - f_{0.2}}{f_{max} - f_{0.2}}\right)^{n_{0.2,max}} + \dfrac{f_{0.2}}{E_{0.2}} + 0.002 & \text{otherwise} \end{cases} \quad (1)$$

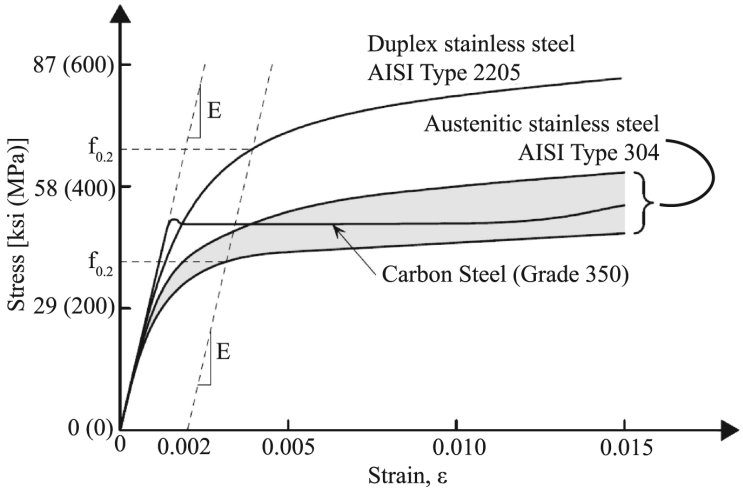

Fig. 1. Typical stress-strain curves of carbon and stainless steels (Dundu, 2018).

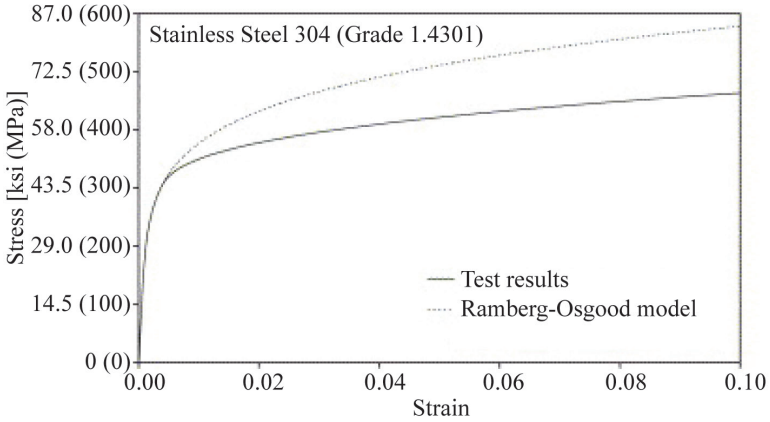

Fig. 2. Comparison of modified Ramberg-Osgood model and experimental stress-strain curves (Ashraf et al., 2006).

where ε is the current strain, f is the current stress, $f_{0.2}$ is the 0.2% offset yield stress, E_0 is the initial modulus of elasticity, n is the strain hardening exponent, $E_{0.2} = \frac{E_0}{1+0.002nE_0/f_{0.2}}$ is the tangent modulus of elasticity at $f_{0.2}$, f_{max} is the maximum reference stress, ε_{max} is the maximum reference strain, and $n_{0.2,max}$ is the Ramberg-Osgood strain-hardening coefficient for the second stage.

Compression Testing

The buckling behavior of concentrically loaded angles has been studied for a number of years. The majority of research has been conducted on carbon steel equal-leg angles. Some research has been conducted on carbon steel unequal-leg angles and stainless steel equal-leg angles. Research on stainless steel unequal-leg angles was not found in the literature search.

Stainless Steel Equal-Leg Angles

In recent years, research on stainless steel equal-leg angles subjected to uniform compression has become an active topic. Before this, Kuwamura (2003) and Sun et al. (2019) provided some of the limited relevant results. Kuwamura was primarily concerned with the local buckling behavior of thin-walled stainless steel sections. As part of that study, 12 cold-formed austenitic equal-leg angle stub columns were tested to failure with nominally fixed-fixed end conditions. Flexural-torsional buckling was observed at failure of the columns with nonslender cross sections having ultimate loads greater than the yield strength of the column (F_yA_g). As the slenderness of individual legs increased, the buckling load decreased and was found to be less than the yield strength for slender legs. Sun et al. investigated hot-rolled stainless steel equal-leg angles subjected to constrained bending where two angles were tested as a pair, clamped together at the quarter points with a spacer, to limit rotation. Of particular interest from this work, Sun et al. completed a series of stub column tests on 9.5 and 12 in. members to obtain material properties. All 10 tests were also found to fail by flexural-torsional buckling with most exceeding the nominal yield strength.

Reynolds (2013) investigated the behavior of laser-welded duplex equal-leg angles. Thirty-three specimens were subjected to concentric compression with the ends pinned for weak-axis bending, fixed for strong-axis bending, and fixed for warping. Weak-axis flexural buckling was observed in 28 of the specimens, while the remaining 5 were found to exhibit flexural-torsional buckling. Considering a draft version of the first edition of the AISC Design Guide 27 (Baddoo, 2013), Reynolds found that the evaluation of flexural-torsional buckling design provisions, which existed in that draft, resulted in overly conservative results, while the accuracy of flexural buckling provisions varied among different specifications. A parametric study using shell finite elements indicated the flexural-torsional buckling became increasingly critical as the cross-section slenderness increased.

Liang et al. (2019) subjected 16 fixed-ended hot-rolled austenitic stainless steel equal-leg angles to concentric compression. All members depicted flexural-torsional buckling, but longer members also incorporated an interaction with flexural buckling. Liang et al. used the experimental results to develop a complementary finite element parametric study. When comparing these results with existing design provisions, flexural-torsional buckling was conservatively predicted. They also compared the results to proposed carbon steel direct strength method provisions for flexural-torsional buckling, which resulted in improved accuracy in terms of capacity. However, approximately half of the estimated direct strength method capacities were unconservative due to not accounting for the softer material response of stainless steel relative to carbon steel. A comparable study completed by Sirqueira et al. (2020) with 18 fixed-ended, hot-rolled, austenitic stainless steel equal-leg angles obtained similar conclusions. Additional numerical work with slender-element equal-leg angles noted that observed local buckling did not correspond with the behavior indicated by the Eurocode 3 provisions (Sarquis et al., 2020).

An extended series of compression tests were completed at the University of Belgrade, including hot-rolled (Filipović et al., 2021a), laser welded (Filipović et al., 2021b), and cold-formed (Dobrić et al., 2020) stainless steel equal-leg angles. All columns were fixed for strong-axis bending and torsion while pinned for weak-axis bending. The measured yield strength was consistently found to exceed the specified nominal value with the largest variation of 55% noted for the hot-rolled sections. The shorter stub column tests were found to fail in flexural-torsional buckling. The slender-element cold-formed section exhibited failure below the yield stress, while the laser welded and hot-rolled specimens exceeded the yield stress. Flexural-torsional buckling was observed throughout the shorter specimens with a gradual transition to flexural buckling behavior at long lengths. The test results indicated that existing design procedures in the Eurocode and the first edition AISC Design Guide 27 (Baddoo, 2013) resulted in safe, but inaccurate strength predictions. For the AISC calculations, only flexural buckling was considered as recommended in the first edition of the AISC Design Guide 27. Another test series of 24 hot-rolled, stainless steel equal-leg angles, including short and long member lengths studied by Zhang, Y., et al. (2020; 2021), observed similar global buckling behaviors and inaccurate strength predictions by the Eurocode and AISC Design Guide 27 design procedures.

Table 1. Flexural Buckling Coefficients for Stainless Steel (AISC, 2021)					
Member Type	**Curve**	α	β_0	β_1	β_2
Rolled or built-up I-shaped sections buckling about the minor axis, and other sections not specified in this table	A	0.56	0.759	0.409	0.690
Rolled or built-up I-shaped sections buckling about the major axis, welded box sections, and round HSS	B	0.58	0.891	0.455	0.820
Rectangular HSS	C	0.69	1.195	0.501	0.820

Behzadi-Sofiani et al. (2021) completed an experimental and numerical study on fixed-ended stainless steel equal-leg angle columns. The flexural buckling controlled capacities were reasonably estimated using existing Eurocode design provisions, but flexural-torsional buckling controlled design predictions varied significantly ranging from near capacity to less than 20% of the expected strength. They noted that current Eurocode flexural-torsional buckling design procedures effectively double counted the reduction in strength from flexural-torsional buckling and local buckling as the two phenomena are mechanically equivalent in equal-leg single angles.

Unequal-Leg Angles

Despite the growing database for equal-leg angles, only minimal published research on unequal-leg angles subjected to uniform compression was located, and none for stainless steel members. Early work by Liu and Chantel (2011) considered 26 carbon steel unequal-leg angles subjected to compression with varying amounts of eccentricity. All five concentrically loaded angles failed primarily in flexural buckling at less than 40% of the yield stress. Dinis et al. (2015) evaluated four carbon steel unequal-leg angles to investigate the elastic flexural-torsional response in asymmetric sections. Experimental results and subsequent modeling were in agreement with the standard theoretical elastic buckling capacity used in the AISC *Specifications*. Ojalvo (2011) summarized the results of three fixed-end aluminum unequal-leg angles tests (Liao, 1982; Wu, 1982). The inelastic response of the fixed-ended columns captured additional post-critical strength excluded in standard elastic buckling assumptions. Recently, Y. Zhang and colleagues (2020, 2021) tested a combined 22 pinned-end aluminum unequal-leg angle columns. Experimental results consistently exhibited flexural-torsional buckling. The response was dominated by torsional behavior at short lengths with a gradual transition to significant flexural behavior at long lengths.

Design Provisions

In the late 1800s, Engesser demonstrated how inelastic buckling capacity could be determined by considering the tangential stiffness of a perfectly straight column, which was in agreement with experimental results (Timoshenko and Gere, 1961). This approach still serves as the basis behind current methods included in AISC 370 (2021). These provisions capture this phenomenon by converting the elastic buckling stress, F_e, into the critical buckling stress, F_{cr}, using a three-stage response. Similar to carbon steel, low compressive stresses correspond to an elastic buckling behavior with a minor reduction for member imperfections. As the stress increases, the response transitions to include inelastic buckling behavior. Unlike carbon steel, designs with stainless steel allow for full yield in compression at short lengths. Based on existing research, Meza et al. (2021) developed the current flexural design provisions for compression members, given by Equation 2:

$$F_{cr} = \begin{cases} F_y & \text{if } \dfrac{F_y}{F_e} \le \left(\dfrac{\beta_0}{\pi}\right)^2 \\ 1.2\left[\beta_1^{\left(\frac{F_y}{F_e}\right)^{\alpha}}\right]F_y & \text{if } \left(\dfrac{\beta_0}{\pi}\right)^2 < \dfrac{F_y}{F_e} \le 3.20 \\ \beta_2 F_e & \text{if } \dfrac{F_y}{F_e} > 3.20 \end{cases} \quad (2)$$

where α, β_0, β_1, β_2 are flexural buckling coefficients that vary based on the member type as shown in Table 1. Multiple column curves have been adopted to capture the increased strength associated with different cross sections buckling.

When applying AISC 370, single-angle compression member design is currently limited to equal-leg, nonslender cross sections. Despite the buckling coefficients being based on flexural buckling, the design procedures require the determination of the minimum controlling elastic global buckling behavior, including flexural-torsional buckling, which is then adjusted using Equation 2 with Curve A coefficients from Table 1. The singly symmetric geometry of equal-leg angles normally exhibits flexural buckling about the weak axis at longer lengths with a transition to flexural-torsional buckling at short lengths. This transition is typically associated with a significant drop in buckling capacity compared to the flexural buckling response. While

Table 2. Experimental Mechanical Properties					
Specimen	E_0 (ksi)	f_y (ksi)	$f_{1.0}$ (ksi)	n	$n_{0.2,1.0}$
C-1-A	28750	52.6	64.7	5.35	2.57
C-2-B	27780	38.9	50.9	4.23	2.20
C-3-C	28350	43.4	46.2	10.45	1.51
C-4-A	25760	54.9	63.5	8.78	2.12
C-5-A	27800	54.5	62.3	9.13	2.55
C-6-B	27760	46.1	53.7	8.83	2.29
Average	27700	48.4	56.9	7.80	2.21

not covered by the AISC 370, an asymmetric unequal-leg angle would behave similarly, in that flexural behavior dominates at long lengths, which then transitions to torsional dominated behavior at short lengths. However, the controlling response is always a flexural-torsional buckling, which means there is consistently an additional reduction applied to the buckling capacity.

An interesting phenomenon in single angles is the equivalency of flexural-torsional buckling and local buckling, both in terms of the deformed shape and buckling capacity for equal-leg angles (Rasmussen, 2005; Behzadi-Sofiani et al., 2021). As a result, existing design provisions run the risk of double counting the same effect when evaluating flexural-torsional buckling and local buckling in single angles. This issue is addressed in AISC 360 for carbon steel members (AISC, 2022) by not requiring the consideration of flexural-torsional buckling in compression member design for most single angles, except if they are very slender cross sections. Galambos (1991) demonstrated that carbon steel single angles, both equal-leg and unequal-leg cross sections, could safely be designed using the flexural buckling capacity reduced for local buckling concerns. This provision was carried forward to the first edition AISC Design Guide 27 (Baddoo, 2013) as it was modeled after AISC 360 with additional reductions for the nonlinear behavior of stainless steel. However, that exception was not incorporated into the current AISC 370 or second edition AISC Design Guide 27 (Baddoo and Meza, 2022).

EXPERIMENTAL DATA

This computational study utilized the hot-rolled stainless steel unequal-leg angle compression testing program completed at the University of Wisconsin-Madison (Laracuente et al., 2022; Laracuente, 2022; Laracuente et al., 2023). As part of the preliminary investigation, the stress-strain behavior of the Gr. 304 stainless steel angles was measured via six tensile coupon tests. The coupons, C, were labeled with the overall test numeric identifier and a second letter based on the position around the cross section as illustrated in Figure 3. Table 2 summarizes the best fit of the experimental results using a two-stage modified Ramberg-Osgood model using a 1% maximum strain as reference point in line with Arrayago et al. (2015).

The main experimental series evaluated 18 hot-rolled stainless steel L3×2×¼ columns, which included three nominally identical specimens, each at six different lengths. Each specimen, S, was given a unique name that identifies the nominal length in inches and a numeric identifier. Prior to testing, the dimensions of the angles were measured by hand. Table 3 summarizes the measured dimensions, where L is the length of the specimen; b and h are the width and height of the section, respectively; and t_b and t_h are the corresponding leg thicknesses as depicted in Figure 4. The imperfections along the length of the specimen were measured using noncontact laser methods (Laracuente et al. 2022; Sippel, 2022) with the maximum imperfections

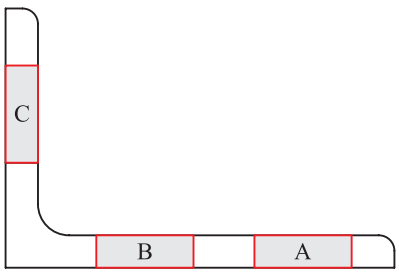

Fig. 3. Coupon position around cross section.

Table 3. Measured Geometric Properties of Test Specimens						
Specimen	L (in.)	b (in.)	h (in.)	t_b (in.)	t_h (in.)	Area (in.^{2})
S10-1	10	2.049	2.979	0.257	0.266	1.251
S10-2	10	2.055	2.977	0.258	0.243	1.191
S10-3	10	2.052	2.966	0.258	0.244	1.192
S20-1	20	2.030	2.981	0.253	0.253	1.203
S20-2	20	2.063	2.958	0.258	0.241	1.182
S20-3	20	2.063	2.965	0.259	0.243	1.190
S36-1	36	2.019	2.985	0.251	0.253	1.198
S36-2	36	2.014	2.991	0.251	0.253	1.198
S36-3	36	2.076	2.964	0.259	0.241	1.190
S72-1	72	2.005	2.987	0.250	0.250	1.185
S72-2	72	2.010	2.985	0.251	0.249	1.184
S72-3	72	2.034	2.980	0.253	0.256	1.214
S100-1	100	2.057	2.957	0.258	0.252	1.210
S100-2	100	2.067	2.933	0.258	0.252	1.208
S100-3	100	2.063	2.939	0.258	0.253	1.209
S148-1	147 15/16	2.006	2.999	0.249	0.254	1.199
S148-2	147 15/16	2.033	2.972	0.256	0.244	1.182
S148-3	147 15/16	2.020	2.989	0.255	0.254	1.210

summarized in Table 4. As illustrated in Figure 4, dx and dy are the lateral imperfection in the x- and y-direction at the heel of the angle, and $d\theta$ is the rotation of the cross section.

Compression Tests

The full-scale compression tests were conducted using a Southwark Emery Testing Machine with a 1-million-pound capacity. As illustrated in Figure 5, the tests were completed with nominal fixed-fixed boundary conditions using reusable ASTM A572/A572M Gr. 50 (2021) carbon-steel top and bottom bearing plates. Before starting the test series, the 10×10×1¼ bottom plate, the 14×14×1¼ top plate, and the end of each angle were milled flat to provide full end bearing. Three ¾-in.-thick, ASTM A36/A36M (2019) clamping brackets were then used to laterally position the angle and provide lateral restraint at the base of the member since there was no positive connection to the bearing plates. All test specimens were observed to exhibit flexural-torsional buckling at the failure loads summarized in Table 5. The buckling response was dominated by torsional deformations for short specimens and transitioned to flexural bending for longer specimens.

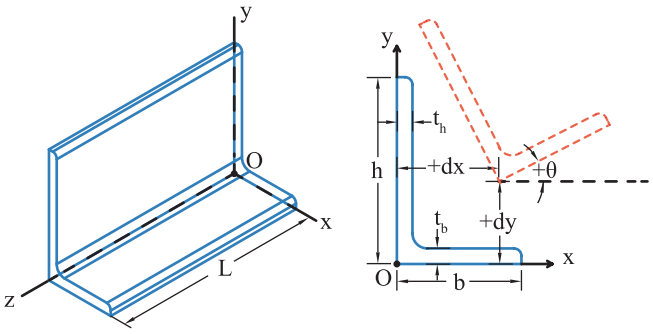

Fig. 4. Unequal-leg angle conventions for dimensions, axes, and displacements.

COMPUTATIONAL STUDY

Modeling Methodology

Using the experimental series just discussed, the modeling approach for an unequal-leg angle was validated before conducting a finite element-based parametric study. The reference L3×2×¼ specimens were evaluated using finite element analysis (FEA) via Abaqus (Dassault Systems, 2015b). The unequal-leg cross sections were modeled as S4R shell elements, which has a four-node linear formulation with reduced integration, hour-glass control, and a general formulation that includes both thick and thin shell behavior (Dassault Systems, 2015a). This approach aligned with previous works (Reynolds, 2013; Liang et al., 2019;

Table 4. Maximum Measured Imperfections						
	Measured			Normalized		
Specimen	*dx* (in.)	*dy* (in.)	θ (deg)	$dx/(L/1000)$	$dy/(L/1000)$	$\theta/\tan^{-1}(L/1000h)$
S10-1	−0.014	−0.007	−0.20	−1.434	−0.705	−1.05
S10-2	0.003	0.002	0.04	0.347	0.197	0.21
S10-3	0.003	0.002	N/A[1]	0.300	0.150	N/A[1]
S20-1	−0.016	−0.013	−0.22	−0.787	−0.639	−0.56
S20-2	−0.006	−0.003	0.04	−0.288	−0.160	0.09
S20-3	0.005	−0.009	0.05	0.236	−0.442	0.13
S36-1	0.018	−0.018	−0.12	0.494	−0.499	−0.17
S36-2	−0.011	−0.036	−0.18	−0.299	−1.000	−0.26
S36-3	−0.048	−0.022	−0.21	−1.339	−0.603	−0.31
S72-1	0.063	−0.064	0.26	0.873	−0.893	0.19
S72-2	−0.142	−0.134	0.15	−1.978	−1.857	0.11
S72-3	0.035	−0.037	0.10	0.483	−0.520	0.07
S100-1	0.218	0.070	−0.30	2.183	0.695	−0.16
S100-2	0.086	−0.073	−0.37	0.858	−0.732	−0.19
S100-3	−0.037	−0.126	0.35	−0.369	−1.259	0.18
S148-1	−0.070	−0.141	−0.20	−0.472	−0.955	−0.07
S148-2	0.470	0.206	−0.33	3.178	1.389	−0.12
S148-3	0.287	−0.070	−0.20	1.943	−0.474	−0.07

[1] Results from scanned data not available due to poor scan quality.

Table 5. Experimental Failure Loads for All Test Specimens					
Specimen	Load (kips)	Specimen	Load (kips)	Specimen	Load (kips)
S10-1	62.1	S36-1	57.1	S100-1	19.2
S10-2	69.5	S36-2	52.7	S100-2	18.4
S10-3	68.8	S36-3	53.3	S100-3	18.0
S20-1	61.3	S72-1	30.8	S148-1	7.8
S20-2	66.8	S72-2	24.8	S148-2	5.6
S20-3	65.4	S72-3	34.4	S148-3	6.7

Sirqueira et al., 2020; Behzadi-Sofiani et al. 2021; Zhang, L., et al., 2019, 2020, 2021; Dinis et al., 2015; de Menezes et al., 2019) that have shown shell elements can be used to accurately model single angles in compression.

The unequal-leg geometry was modeled using the centerline model shown in Figure 6(b) using centered elements, which has been shown to provide similar computational results compared to solid element models (Reynolds, 2013; Dinis et al., 2015). Based on a refinement study, the member was modeled using a square mesh with 16 elements across the short flange with equivalent sized elements on the long flange as indicated in Figure 6(c). The end boundary

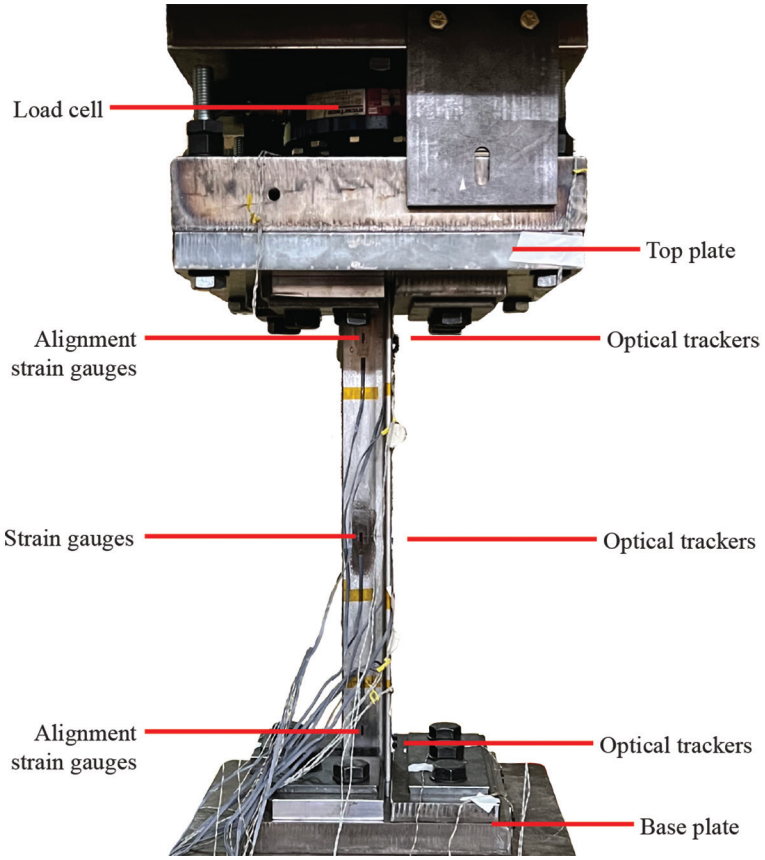

Fig. 5. Typical compression testing setup.

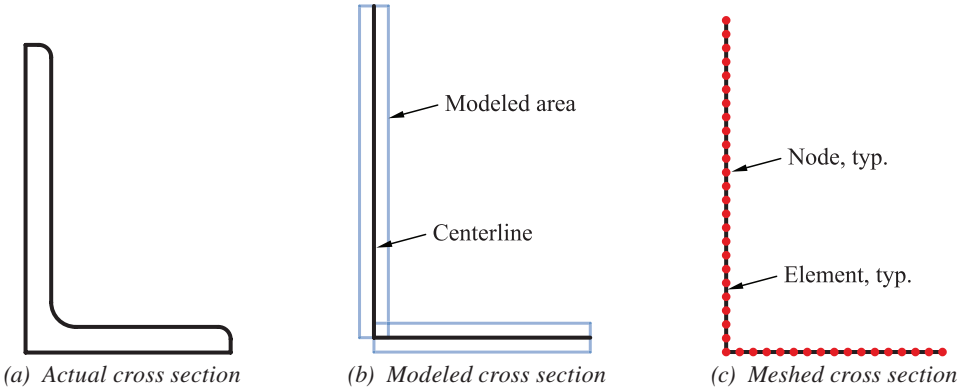

Fig. 6. Typical model of unequal-leg cross section.

Table 6. Imperfection Distributions Considered in the Validation Study				
	Translations		Rotations	
Label	Smooth	Sine	Smooth	Sine
IV-1	×			
IV-2	×		×	
IV-3	×			×
IV-4		×		×

condition for the unequal-leg angle models was applied using a single reference node at the angle centroid that was connected to all nodes across the end of the angle through a rigid tie constraint. As a result, the angle ends were always fully constrained against warping, and the flexural boundary condition could be readily defined as fixed or pinned in the geometric orientations. For the validation analysis, the end of the member was fixed for bending about both axes.

The material model for this study was selected from the experimental results listed in Table 2. Evaluating the axial response of the 10 in. columns, which correspond to typical stub column test geometry, stress-strain curve 5 (C-5-A) from Table 2 was selected as it best captured the ultimate capacity, initial modulus of elasticity, and intermediate stiffness as depicted in Figure 7. Due to the variable stress-strain behavior captured within each leg in the initial coupon tests, this comparison included the average strain result at the middle of each leg to confirm that the selected model was appropriate for both legs. This behavior was implemented in the finite element analysis using an elastic-plastic model that ignored the initial (0.5 ksi)/E_0 plastic strain to minimize the concerns of underestimating capacity noted by Schafer et al. (2010).

Four variations of the measured imperfections were evaluated, as summarized in Table 6, where IV represents imperfection variation, to investigate the effect of the imperfection shape. Rotation and translations were treated as distributions that could be separately applied to determine the importance of including the rotation imperfection that is occasionally excluded in parametric studies. Additionally, the imperfection profile was applied as a "Smooth" or "Sine" profile as shown in Figure 8. The Sine profile applied a traditional half-sine curve profile based on the maximum imperfection value noted in Table 4. The Smooth profile accounted for the variable imperfection along the length of the specimen. The profile was interpolated from the measured profile to fit the underlying finite element mesh. This process included a smoothing filter to eliminate localized kinks that created unrealistic stress concentrations.

Validation Results

The results of the validation study are provided in Table 7. The computational models matched well with the experimental results for all specimens 72 in. and shorter. The finite element analysis was able to replicate the torsional buckling dominant response in short columns as shown in Figure 9. The inclusion of additional flexural movement as the column length increased was also captured as depicted in Figure 10. However, as the buckling transitioned to a

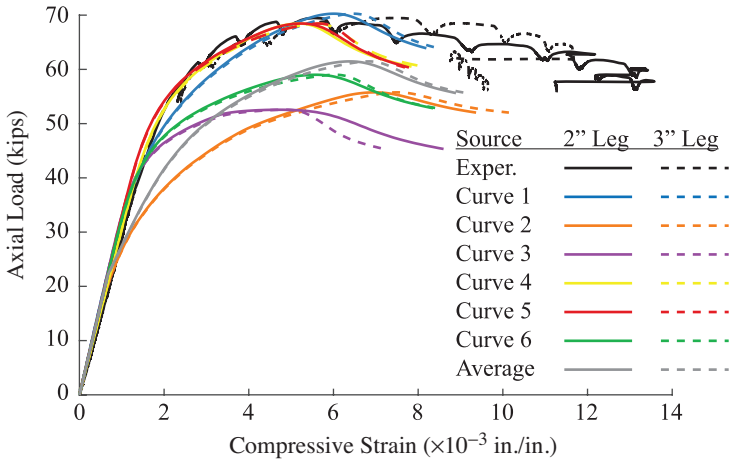

Fig. 7. Applied axial load-strain response of S10-2 column.

Table 7. Ultimate Failure Loads for Validation Modeling with Variable Imperfections					
Specimen	Test (kips)	Ultimate Load (kips) with IV-1	IV-2	IV-3	IV-4
S10-1	62.1	70.3	69.5	69.5	69.6
S10-2	69.5	68.9	68.4	68.4	68.4
S10-3	68.8	69.1	69.1	69.1	69.1
S20-1	61.3	62.0	61.4	61.5	61.6
S20-2	66.8	63.4	63.5	63.6	63.3
S20-3	65.4	63.5	63.5	63.3	63.0
S36-1	57.1	53.0	53.1	53.2	53.7
S36-2	52.7	54.4	54.0	53.9	52.9
S36-3	53.3	51.7	51.3	51.4	51.3
S72-1	30.8	33.2	33.0	32.9	33.4
S72-2	24.8	28.3	28.3	28.4	28.4
S72-3	34.4	35.1	35.1	35.0	36.7
S100-1	19.2	19.1	19.1	19.1	19.2
S100-2	18.4	22.9	22.9	23.0	22.9
S100-3	18.0	22.4	22.6	22.7	22.2
S148-1	7.8	10.4	10.4	10.4	10.2
S148-2	5.6	9.1	9.1	9.1	9.0
S148-3	6.7	9.9	9.9	9.9	9.9
Full series	**Mean**	1.12	1.12	1.12	1.12
	CoV	0.17	0.17	0.17	0.17
0 in.–72 in. series	**Mean**	1.02	1.02	1.02	1.02
	CoV	0.06	0.06	0.07	0.07

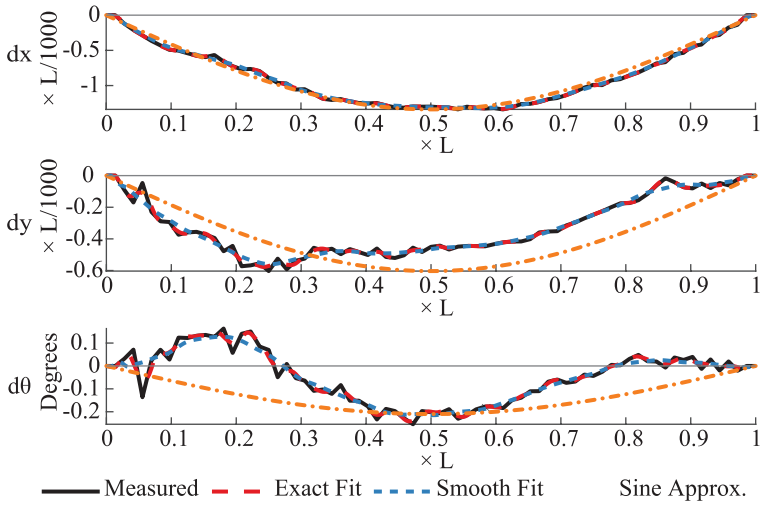

Fig. 8. Initial imperfections as adjusted for finite element modeling for S36-3.

primarily flexural buckling response at long lengths, significant variations between the modeled and actual response were noted. The FEA captured the overall behavior, but at higher magnitudes than the experimental results, as shown in Figure 11.

While investigating the deviation noted in the FEA results for longer specimens, it was observed that the larger flexural deformation of the buckled column combined with the fixed boundary condition caused tension to develop at the end of the specimens in the finite element analysis. While reasonable, this behavior was not possible in the existing test setup because bearing would be lost if tensile flexural stresses exceeded the axial compression. Exploratory work to directly account for contact at the base plate confirmed that uplift did occur at buckling for the longer specimens due to the lack of a positive connection to the bearing plate. It was found that the angle lifted at the heel, which increased the bearing stress at the tip, causing more localized yielding of the angle as shown in Figure 12. The loss of bearing was not visually confirmed during testing due to the lateral clamping plates, but the direction the angle moved while buckling corresponded with the tensile stresses at the heel from bending. The FEA results with contact exhibited a reduced ultimate capacity and less post-buckling

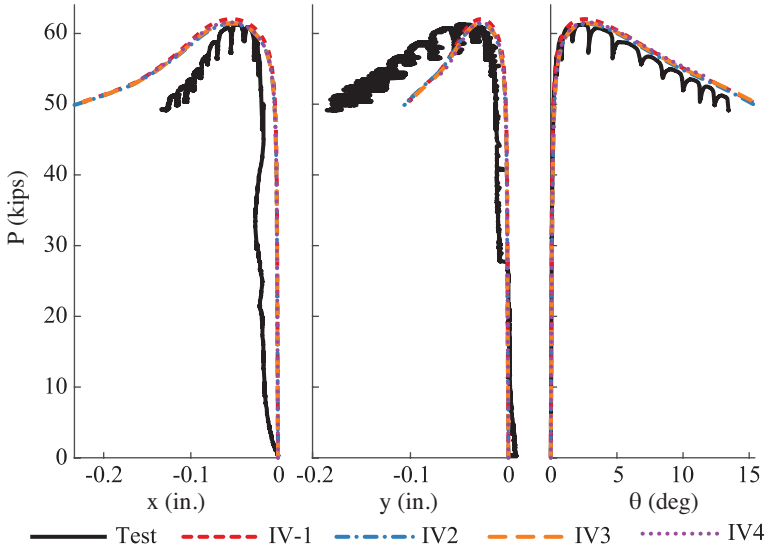

Fig. 9. Torsion dominated buckling displacement of S20-1.

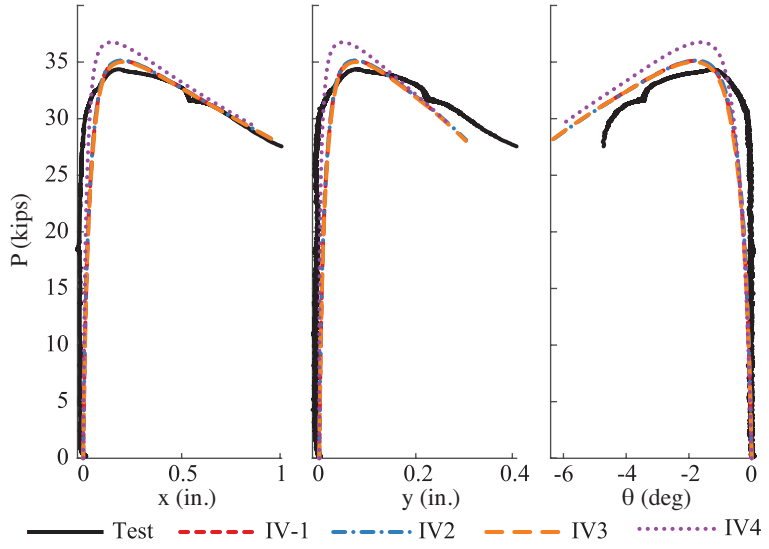

Fig. 10. Intermediate flexural-torsional buckling displacement of S72-3.

ductility from the perfect support, but not enough to match the experimental results.

Upon closer inspection of the base plates after the compression tests, it was noted that there was permanent deformation as shown in Figure 13. While it was not anticipated that the base plates would plastically deform under ultimate loads based on the nominal stainless steel yield strength, the actual experimental yield strength of the angles was measured as 60% greater than nominal (Laracuente et al., 2022), which caused small impressions on the base plates under the tips of each angle leg. While the high stresses of the short columns affected the entire bearing area, the primary concern was the tips of each leg where roughly the end 0.6 in. of each leg was clearly deformed, varying approximately linearly to a max impression of 0.02 in. at the tip.

Due to these observations, the finite element model was refined to account for the imperfect base plate. The base plate was modeled as a solid body with a perfectly elastic-perfectly plastic response accounting for the nominal 50 ksi yield strength. The angle and base plate were modeled with contact and allowed to separate under tension. Initial investigations utilized a perfect rectangular cube for the base plate geometry, but later variations considered existing initial imperfections by utilizing a trapezoidal profile as shown in Figure 14. Multiple profiles were considered to address the limitations in defining the exact geometry of the indentations. This modeling incorporating contact, the imperfect bearing surface, and deformation of the base plate resulted in only minor changes for shorter columns; however, the majority of 100 and 148 in. models captured a significantly reduced capacity, as shown in

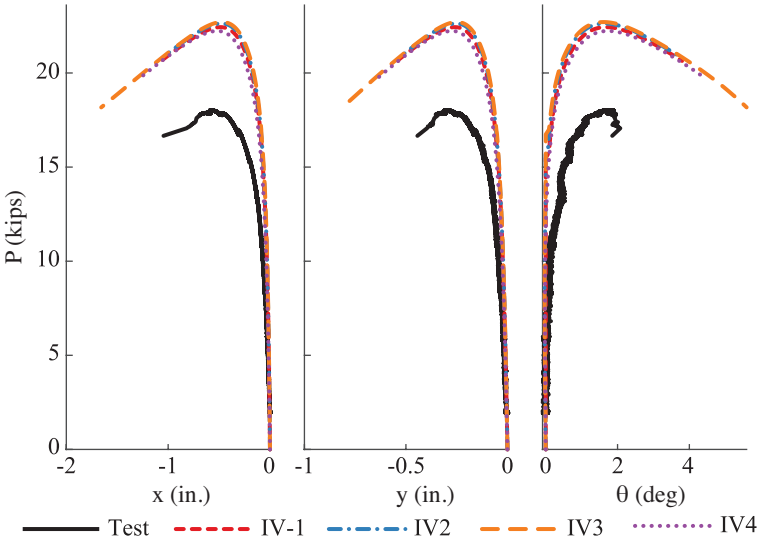

Fig. 11. Flexure dominated buckling displacement of S100-3.

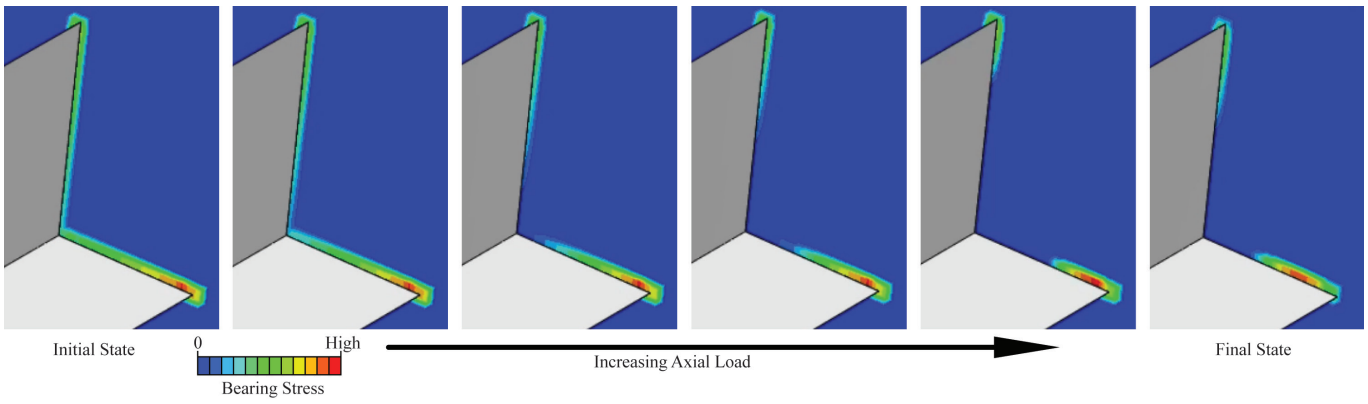

Fig. 12. Typical changes in bearing stress when allowing for uplift of angle specimen at support.

Figure 15; less overall deflection at ultimate capacity; and partial bearing, which occurred with both the perfect cube or modified deformed base plate geometry. These results indicated that the longer-length specimens were sensitive to the bearing support condition and, therefore, explained the discrepancy between the experiments and modeling results. The validation study demonstrated that the modeling approach was capable of depicting the behavior of stainless steel unequal-leg angles with perfect boundary conditions, and thus was acceptable to implement in a FEA-based parametric study.

PARAMETRIC STUDY

A parametric study was conducted to expand the available data for unequal-leg single angles. In total, 12 representative nonslender, unequal-leg angle cross sections, listed in Table 8, were selected to cover typical h/t, b/t, and h/b ratios of the 50 nonslender-element cross sections that are currently available for purchase or listed in the AISC *Steel Construction Manual* (AISC, 2017).

Each cross section was evaluated with nominal dimensions; nominal imperfections; and an effective slenderness ratio, L_e/r_z, ranging from 5 to 200. The nominal imperfections were half-sine wave imperfections with a magnitude of L/1000 in the negative x- and y-directions and a rotation of $-\tan^{-1}L/(1000h)$, but limited to 1°. All cross sections were modeled for both a fixed-fixed, $L_e = 0.5L$, and pinned-pinned, $L_e = 1.0L$, boundary condition. The angles were then modeled with either the measured material properties, matching the validation study, or nominal material properties for 304 or 304L based on AISC 370 nominal values (2021) listed in Table 9. These parameters created 960 models that were evaluated for each of the three material models, resulting in a total of 2,880 models. In these models, flexural-torsional buckling was consistently observed. Similar to the experimental results, flexural deformations were dominant at high slenderness ratios, and as the slenderness ratio decreased, torsional deformations became more dominant. Due to the selected imperfection, a few geometries displayed a deviation from the typical flexural buckling response as shown in Figure 16; however, this consistently

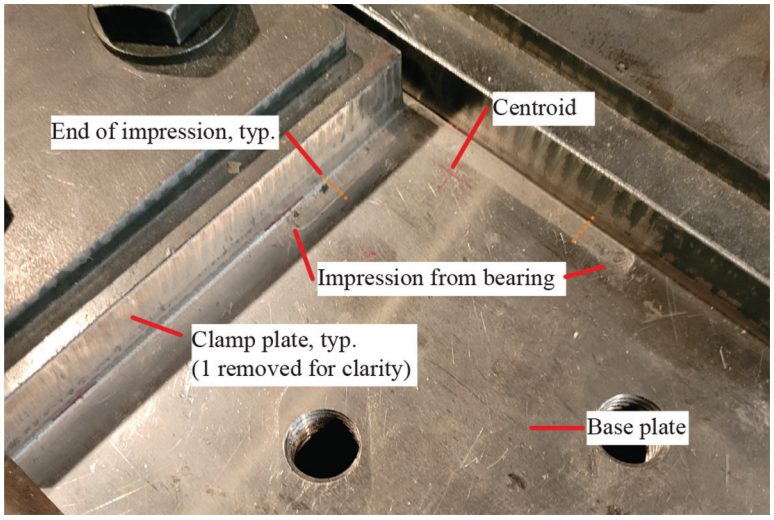

Fig. 13. Base plate after final compression test series.

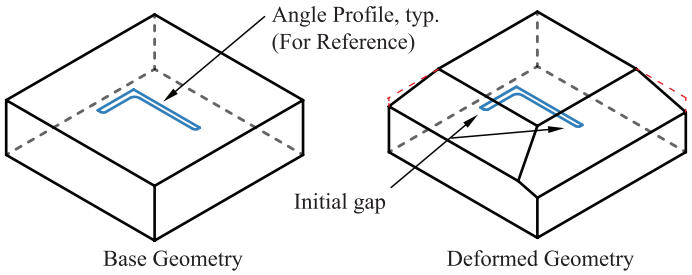

Fig. 14. Base plate geometry (not to scale).

Table 8. Angles in Parametric Study			
Section	*h*/*t*	*b*/*t*	*h*/*b*
L1½×1¼×⅛	12.0	10.0	1.20
L2×1×¼	8.0	4.0	2.00
L2×1½×¼	8.0	6.0	1.33
L3×1½×¼	12.0	6.0	2.00
L3×2×¼	12.0	8.0	1.50
L3×2×⅜	8.0	5.3	1.50
L4×3×⅜	10.7	8.0	1.33
L4×3×½	8.0	6.0	1.33
L5×3×½	10.0	6.0	1.67
L6×3×½	12.0	6.0	2.00
L6×4×½	12.0	8.0	1.50
L6×5×½	12.0	10.0	1.20

Table 9. Nominal Material Properties					
Grade	*E* (ksi)	f_y (ksi)	f_u (ksi)	*n*	*m*
304	28000	30	75	7	2.12
304L	28000	25	70	7	2

corresponded with an increase in capacity relative to the design flexural buckling curve, not the decrease typically associated with including flexural-torsional buckling.

The initial parametric study comparison, shown in Figures 16 and 17, considered all three AISC 370 flexural buckling curves as identified previously in Equation 2 and Table 1. If unequal-leg angles were covered by AISC 370, the section would be evaluated with Curve A values. The other alternatives were included to investigate whether the capacity increase associated with Curves B or C could be considered for unequal-leg angles as the section has not been thoroughly investigated.

DISCUSSION

As shown in Figure 17 [see Sippel (2022) for plots of each angle individually], a consistent result of the parametric study was that neither Curve B nor Curve C (refer to Table 1) were conservative estimates of strength for the buckling response. Therefore, the possible increase in

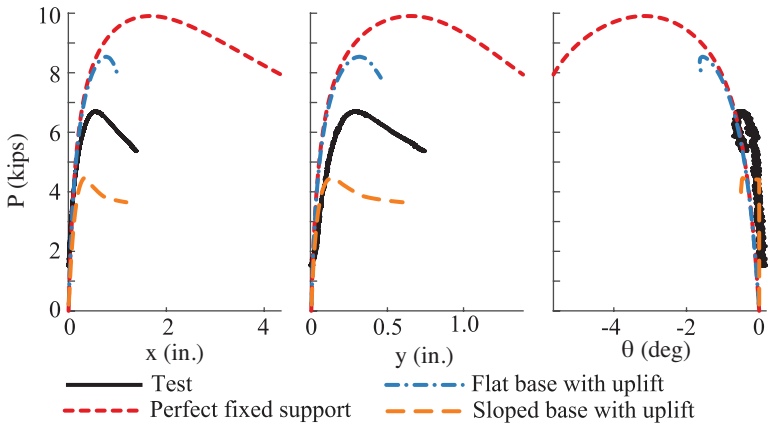

Fig. 15. Effect of changing support on buckling behavior of S148-3.

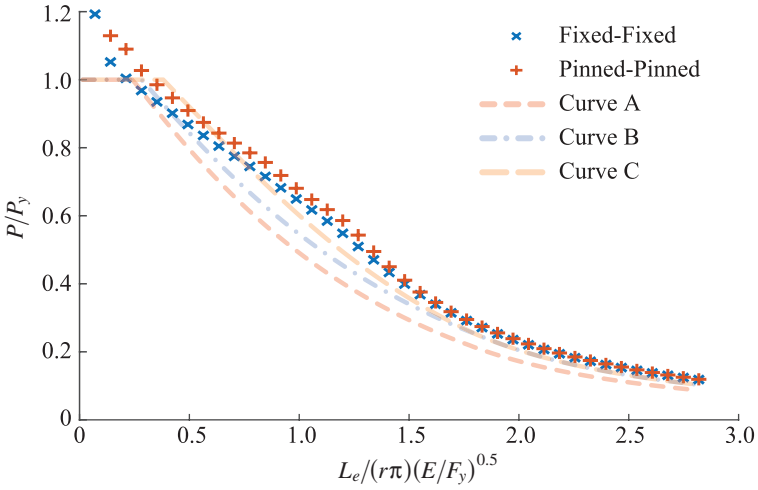

Fig. 16. Buckling behavior of L6×4×½ with measured material properties versus AISC 370 buckling curves using measured yield strength.

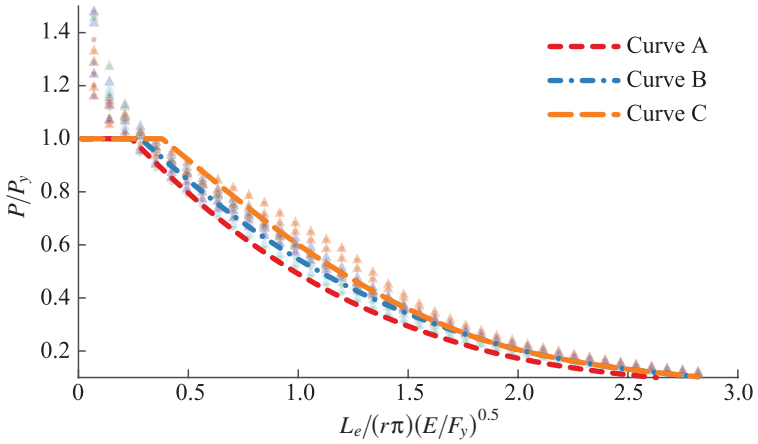

(a) Measured material properties

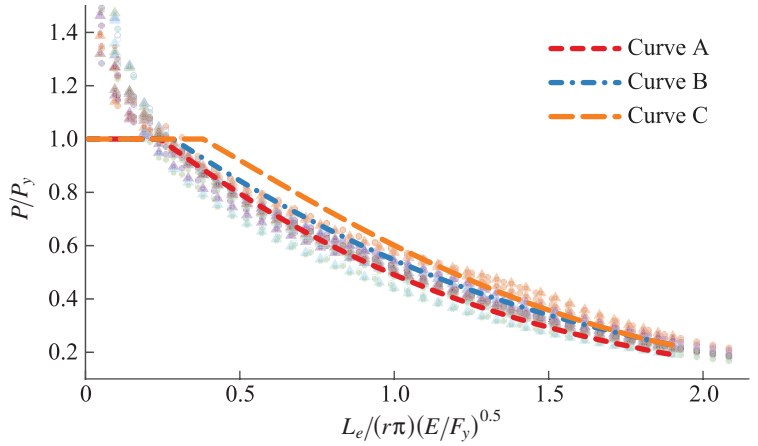

(b) Nominal material properties

Fig. 17. Buckling behavior with different material properties versus AISC 370 buckling curves using corresponding yield strength. All sizes from Table 8 included.

capacity associated with these curves was deemed unlikely, and the remainder of this study focused on comparisons to buckling capacities calculated using Curve A, the applicable parameters for single equal-leg angles. The parametric study showed different behavior depending on the material properties considered. The FEA results with measured material properties were found to be normally greater than Curve A [Figure 17(a)], while a number of FEA results with nominal material properties were lower than Curve A [Figure 17(b)]. By comparing the effective stiffness included in each model in Figure 18, there is a distinct variation between the nominal assumed material behavior, AISC 370-304 and AISC 370-304L, and the measured material behavior, Measured 304. The increased strain-hardening coefficient, n, from the measured material properties in this study, which agrees with previous research on hot-rolled sections (Behzadi-Sofiani et al., 2021; Liang et al., 2019; de Menezes et al., 2019; Sun et al., 2019), caused a stiffer material response.

This dissimilarity of results within the parametric study between FEA with measured and nominal material properties is further highlighted when comparing the simulated FEA column capacity, P_{SIM}, to the compression capacity from AISC 370 design provisions with the corresponding yield strength and considering flexural buckling, P_{FB}, or flexural-torsional buckling, P_{FTB}—that is, Figure 19 normalizes the FEA results from nominal material properties with buckling capacities based on the nominal yield strength, and Figure 20 normalizes the FEA results from measured material properties with buckling capacities calculated using the measured yield strength. For the nominal material properties with results summarized in Figure 19, the flexural buckling capacity alone was observed to underestimate the capacity of multiple sections at shorter lengths [Figure 19(b)]. Including flexural-torsional buckling effects caused the buckling capacity to be reduced for all cross sections, which included a maximum change between 5% and 24%. As shown in Figure 19(a), this change resulted in a conservative estimate in all cross sections except for the pinned L2×1×¼ and L5×3×½ columns. This contrasts with the measured material property results, Figure 20, that indicate that flexural buckling alone was an adequate predictor of strength [Figure 20(b)]. Note that the unconservative results using the flexural buckling prediction would be eliminated in most instances, except for a narrower range of the same pinned L2×1×¼ and L5×3×½ columns if local buckling was considered, which is shown in Figure 20(c). The measured yield strength would reclassify some cross sections as slender.

The varied results of the parametric study highlighted the importance of correctly defining the material properties and stress-strain response for the advanced FEA. With carbon steel sections, the majority of steel grades used for structural design exhibit a consistent material behavior that is readily simplified to an approximate elastic-plastic response. Despite a simple, consistent material model, multiple compression design curves have been developed that vary with the cross-section shape being analyzed (Ziemian, 2010). This issue is complicated for stainless steel members because the variability of the nonlinear constitutive relationship adds an additional dimension. The nominal stress-strain relationship has experimental backing that it is appropriate for the baseline behavior of 304/304L stainless steel in a very broad range of applications. However, additional research, including the testing related to this study (Laracuente et al., 2022, 2023), has regularly noted

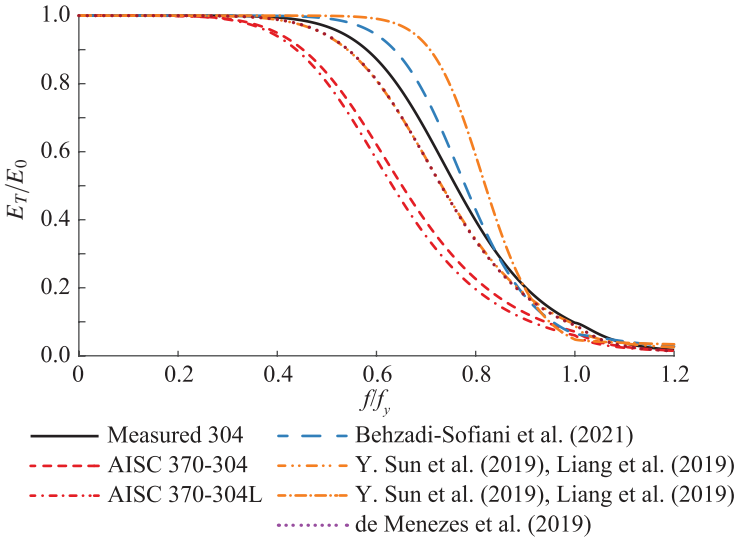

Fig. 18. Effective modulus of elasticity within material models.

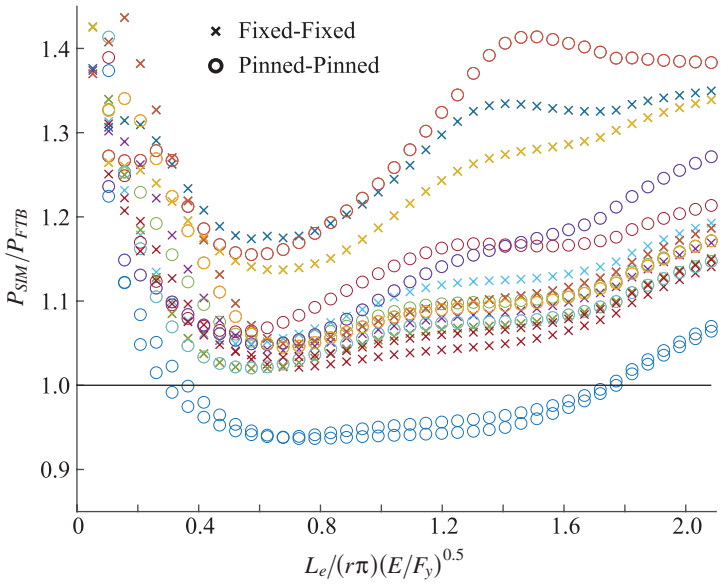

(a) Flexural-torsional buckling design provisions

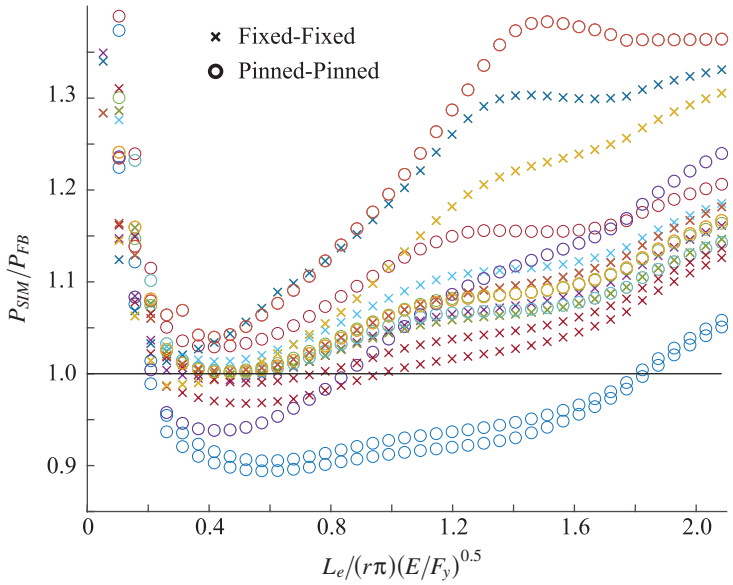

(b) Flexural buckling provisions only

Fig. 19. FEA capacity versus design provision strength calculations with nominal material properties. All sizes from Table 8 included.

significant increases in strength and stiffness when investigating structural stainless steel sections as highlighted in Figure 18. As a result, the three design curves in AISC 370 are attempting to balance the impact of different geometries, including the variable cross sections and typical imperfections as had been done with carbon steel, as well a realistic, average response of typical stainless steel members.

Based on the results of this study, if the nominal AISC material properties are an accurate depiction of a conservative stress-strain relationship and corresponding tangent modulus of elasticity, the design provisions need to include flexural-torsional buckling provisions to determine conservative predictions of capacity in compression. However, if the nominal response is underestimating the tangent modulus of elasticity before yield for typical structural stainless steel sections as observed with the experimental data, the same procedure could result in excessively conservative predictions. Along those lines, an expanded parametric study including slender cross sections and the nominal stress-strain curve would allow for a fundamental understanding of how existing buckling provisions align with the behavior of unequal-leg single angles, which would provide a worst-case design envelope to incorporate them into the specification. Yet, additional investigation into the appropriateness of the nominal stress-strain curve specified in

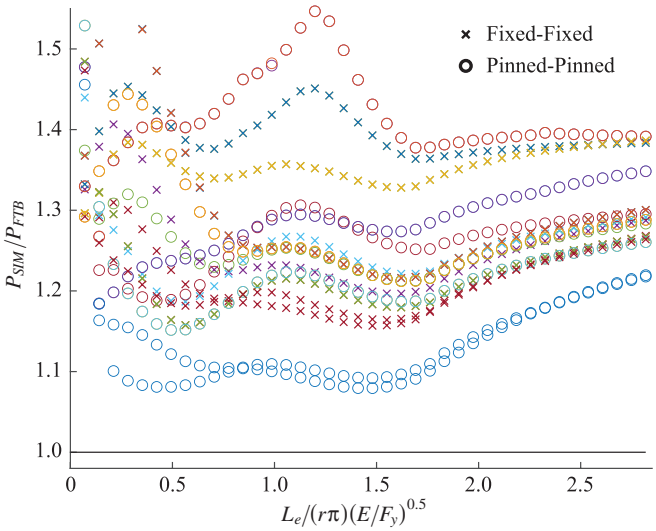

(a) Flexural-torsional buckling design provisions

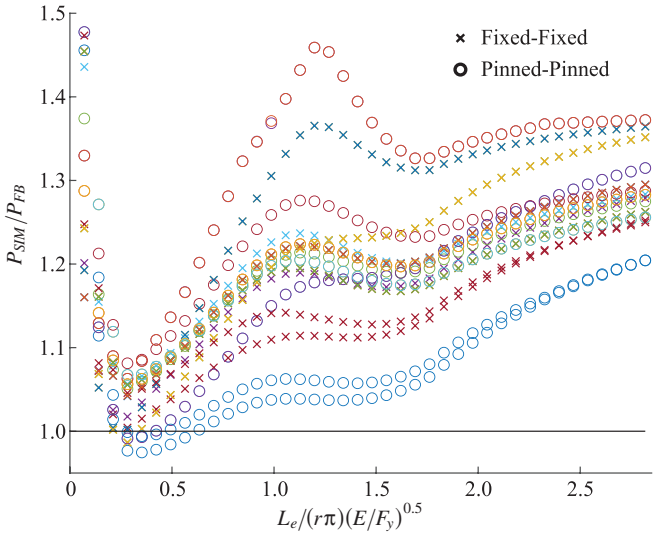

(b) Flexural buckling provisions only

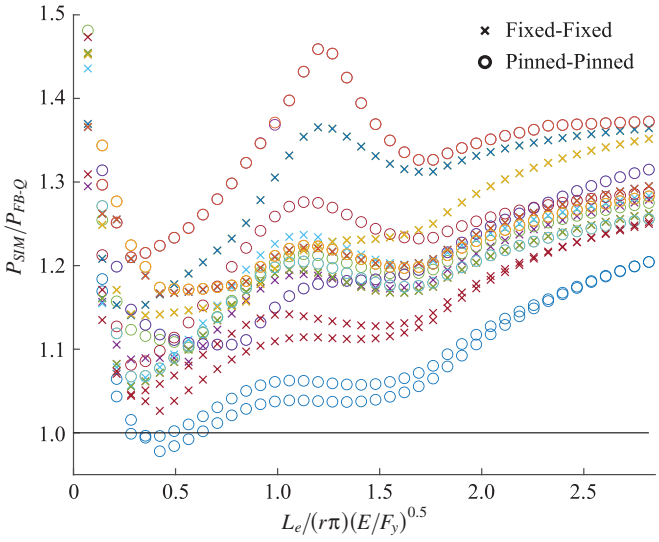

(c) Flexural buckling provisions plus local buckling reductions.

Fig. 20. FEA capacity versus design provision strength calculations with measured material properties. All sizes from Table 8 included.

AISC 370 could warrant later simplifications to the design provisions of unequal-leg angles.

The complex buckling behavior of stainless steel unequal-leg angles makes it difficult to establish a straightforward set of design provisions that accurately predict the true response. A central component of this challenge is accounting for the flexural-torsional buckling response, which is expected to control in all instances, in a form suitable for practicing engineers to apply. The current approach requires consideration of all global elastic buckling modes and then applying the same equations that were developed for flexural buckling to determine the nominal capacity of the column. As currently implemented, the inclusion of flexural-torsional buckling in the design provisions is a significant reduction from the flexural buckling capacity at short lengths as shown in Figure 21. This comparison was completed using the nominal yield strength but follows a similar pattern when using the measured yield strength.

As mentioned previously, this reduction was necessary when using nominal material properties to match finite element simulations. However, the simulations using measured material properties did not need the same reduction despite these models still exhibiting flexural-torsional buckling. When evaluating the same design equations for any global buckling mode, it should be noted that the assumed behavior reflects that the shear stiffness of stainless steel angles reduces proportionally with the longitudinal stiffness, which is not observed in carbon steel for axially loaded members (Galambos, 1991). The consideration of the actual shear stiffness can result in a smaller reduction from flexural buckling to the flexural-torsional response. Based on this reduced difference, not including the global flexural-torsional buckling reduction for carbon steel angles was determined to be acceptable as long as local buckling reductions were included to capture extreme cases of slender cross sections.

Determining the significance of the overestimated capacity requires knowledge of the realistic capacity of single angles. The flexural buckling coefficients given in Curve A were determined to be conservative for the physical stainless steel angles in this study; however, additional data are needed to determine if this is a trend or a unique result. An equivalent investigation can be extended to various stainless steel angle cross sections to consider implementing a similar methodology.

CONCLUSIONS

This study investigated the flexural-torsional buckling behavior of stainless steel unequal-leg single angles. A finite element modeling procedure was developed and validated by comparison to experimental results from 18 fixed-fixed Grade 304 stainless steel L3×2×¼ columns with lengths ranging from 10 to 148 in. The subsequent finite element-based parametric study considered 12 cross sections, nonslender-element for nominal material properties, with a L_e/r_z ratio ranging from 5 to 200 to incorporate elastic and inelastic failures. Each cross section was evaluated for a fixed-fixed and pinned-pinned flexural end restraint and one of three material models: nominal Grade 304, nominal Grade 304L, or the measured material properties determined through the validation study. A total of 2,880

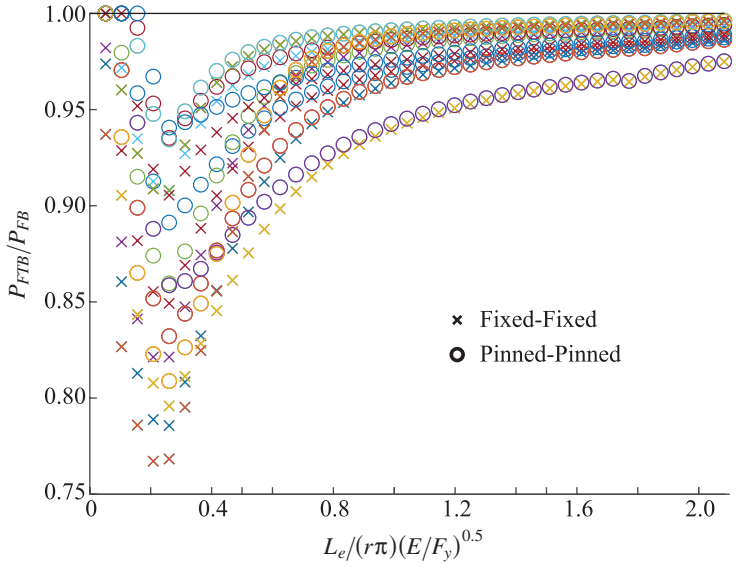

Fig. 21. Current design provision normalized by the flexural buckling only result using nominal material properties. All sizes from Table 8 included.

finite element models were run, and the simulations captured flexural-torsional buckling of all cross sections with both flexural and torsional dominated failures. It was determined that using the existing Curve A buckling coefficients in AISC 370 with nominal material properties required the consideration of flexural-torsional buckling design provisions to obtain results that were consistently conservative compared to the finite element results. Only considering flexural buckling resulted in an average 7% less conservative prediction in the worst-case instance, and half the models exhibited an unconservative prediction. While flexural-torsional buckling was also consistently observed when considering measured material properties, evaluation of the same flexural-torsional buckling design provisions resulted in excessive conservatism for most finite element results with measured material properties. The evaluation of flexural buckling with local buckling reductions, similar to the design provisions for carbon steel single angles, was found to approximate most flexural-torsional buckling concerns for the stainless steel single angles in this part of the study. Additional work should focus on verifying the appropriate stress-strain response for modeling stainless steel and expanding the study to include more slender-element cross sections to validate the consistency of this result and to determine if a limiting element slenderness of the cross section is applicable.

REFERENCES

AISC (2017), *Steel Construction Manual*, 15th Ed., American Institute of Steel Construction, Chicago, Ill.

AISC (2021), *Specification for Structural Stainless Steel Buildings,* ANSI/AISC 370-21, American Institute of Steel Construction, Chicago, Ill.

AISC (2022), *Specification for Structural Steel Buildings,* ANSI/AISC 360-22, American Institute of Steel Construction, Chicago, Ill.

Arrayago, I., Real, E., and Gardner, L. (2015), "Description of Stress–Strain Curves for Stainless Steel Alloys," *Materials & Design,* 87, 540–552. https://doi.org/10.1016/j.matdes.2015.08.001

Ashraf, M., Gardner, L., and Nethercot, D.A. (2006), "Compression Strength of Stainless Steel Cross-Sections," *Journal of Constructional Steel Research*, Vol. 62, No. 1-2, pp. 105–115. https://doi.org/10.1016/j.jcsr.2005.04.010

ASTM (2019), *Standard Specification for Carbon Structural Steel*, ASTM A36/A36M-19, ASTM International, West Conshohocken, Pa.

ASTM (2021), *Standard Specification for High-Strength Low-Alloy Columbium-Vanadium Structural Steel*, ASTM A572/A572M-21, ASTM International, West Conshohocken, Pa.

Baddoo, N. (2013), *Structural Stainless Steel*, Design Guide 27, American Institute of Steel Construction, Chicago, Ill.

Baddoo, N. and Meza, F. (2022), *Structural Stainless Steel*, Design Guide 27, 2nd Ed., American Institute of Steel Construction. Chicago, Ill.

Behzadi-Sofiani, B., Gardner, L., and Wadee, M.A. (2021), "Stability and Design of Fixed-Ended Stainless Steel Equal-Leg Angle Section Compression Members," *Engineering Structures,* Vol. 249, 113281. https://doi.org/10.1016/j.engstruct.2021.113281

Dassault Systems (2015a), *Abaqus 2016 Documentation*. http://130.149.89.49:2080/v2016/index.html

Dassault Systems (2015b), *Abaqus/CAE,* Version 6.16, Dassault Systems, Johnston, R.I.

de Menezes, A.A., da S. Vellasco, P.C.G., de Lima, L.R.O., and da Silva, A.T. (2019), "Experimental and Numerical Investigation of Austenitic Stainless Steel Hot-Rolled Angles under Compression," *Journal of Constructional Steel Research,* Vol. 152, pp. 42–56. https://doi.org/10.1016/j.jcsr.2018.05.033

Dinis, P.B., Camotim, D., Belivanis, K., Roskos, C., and Helwig, T.A. (2015), "On the Buckling, Post-Buckling and Strength Behavior of Thin-Walled Unequal-Leg Angle Columns," *Proceedings of the 2015 SSRC Annual Stability Conference*, Nashville, Tenn.

Dobrić, J., Filipović, A., Marković, Z., and Baddoo, N. (2020), "Structural Response to Axial Testing of Cold-Formed Stainless Steel Angle Columns," *Thin-Walled Structures,* Vol. 156, 106986. https://doi.org/10.1016/j.tws.2020.106986

Dundu, M. (2018), "Evolution of Stress–Strain Models of Stainless Steel in Structural Engineering Applications," *Construction and Building Materials,* Vol. 165, pp. 413–423. https://doi.org/10.1016/j.conbuildmat.2018.01.008

Filipović, A., Dobrić, J., Baddoo, N. R., and Može, P. (2021a), "Experimental Response of Hot-Rolled Stainless Steel Angle Columns," *Thin-Walled Structures,* Vol. 163, 107659. https://doi.org/10.1016/j.tws.2021.107659

Filipović, A., Dobrić, J., Budevac, D., Fric, N., and Baddoo, N. (2021b), "Experimental Study of Laser-Welded Stainless Steel Angle Columns," *Thin-Walled Structures,* Vol. 164, 107777. https://doi.org/10.1016/j.tws.2021.107777

Galambos, T.V. (1991), "Design of Axially Loaded Compressed Angles," *Proceedings of the 1991 SSRC Annual Stability Conference: 'Inelastic Behavior and Design of Frames,'* Chicago, Ill.

Gardner, L. and Ashraf, M. (2006), "Structural Design for Non-Linear Metallic Materials," *Engineering Structures,* Vol. 28, No. 6, pp. 926–934. https://doi.org/10.1016/j.engstruct.2005.11.001

Gardner, L. and Nethercot, D. (2004), "Experiments on Stainless Steel Hollow Sections—Part 1: Material and Cross-Sectional Behaviour," *Journal of Constructional Steel Research,* Vol. 60, No. 9, pp. 1291– 1318. https://doi.org/10.1016/j.jcsr.2003.11.006

Hill, H. (1944), *Determination of Stress-Strain Relations from the Offset Yield Strength Values*, Technical Note 927, National Advisory Committee for Aeronautics, Washington, D.C.

Houska, C. (2014), *Designing Stainless Steel Part 1*, Conference Presentation, NASSC: The Steel Conference, American Institute of Steel Construction, Toronto, ON, Canada.

Hradil, P., Talja, A., Real, E., Mirambell, E., and Rossi, B. (2013), "Generalized Multistage Mechanical Model for Nonlinear Metallic Materials," *Thin-Walled Structures,* Vol. 63, pp. 63–69. https://doi.org/10.1016/j.tws.2012.10.006

Kuwamura, H. (2003), "Local Buckling of Thin Walled Stainless Steel Members," *Steel Structures,* Vol. 3, pp. 191–201.

Laracuente, M.E. (2022), "Behavior of Concentrically Loaded Austenitic Stainless Steel Single Unequal-Leg Angles," Master's Thesis, University of Wisconsin–Madison, Madison, Wis.

Laracuente, M.E., Sippel, E.J., and Blum, H.B. (2022), "Stability Considerations of Unequal-Leg Angle Stainless Steel Columns," *Proceedings of the 2022 SSRC Annual Stability Conference,* SSRC, Denver, Colo.

Laracuente, M.E., Sippel, E.J., and Blum, H.B. (2023), "Stability Considerations of Laser Fused Unequal-Leg Angle Stainless Steel Columns," *Proceedings of the 2023 SSRC Annual Stability Conference*, SSRC, Charlotte, N.C.

Liang, Y., Jeyapragasam, V.V.K., Zhang, L., and Zhao, O. (2019), "Flexural-Torsional Buckling Behaviour of Fixed-Ended Hot-Rolled Austenitic Stainless Steel Equal-Leg Angle Section Columns," *Journal of Constructional Steel Research,* Vol. 154, pp. 43–54. https://doi.org/10.1016/j.jcsr.2018.11.019

Liao, K. (1982), "Compression Tests of Unequal-Leg Angles," Master's Thesis, Ohio State University, Columbus, Ohio.

Liu, Y. and Chantel, S. (2011), "Experimental Study of Steel Single Unequal-Leg Angles under Eccentric Compression," *Journal of Constructional Steel Research,* Vol. 67, No. 6, pp. 919–928. https://doi.org/10.1016/j.jcsr.2011.02.005

MacDonald, M., Rhodes, J., and Taylor, G.T. (2000), "Mechanical Properties of Stainless Steel Lipped Channels," *CCFSS Proceedings of International Specialty Conference on Cold-Formed Steel Structures (1971–2018)*, Session 11, No. 4. https://scholarsmine.mst.edu/isccss/15iccfss/15iccfss-session11/4

Meza, F.J., Baddoo, N., and Gardner, L. (2021), "Development of Flexural Buckling Rules for the New AISC Stainless Steel Design Specification," *ce/papers,* Vol. 4, pp. 1537–1542. https://doi.org/10.1002/cepa.1453

Mirambell, E. and Real, E. (2000), "On the Calculation of Deflections in Structural Stainless Steel Beams: An Experimental and Numerical Investigation," *Journal of Constructional Steel Research,* Vol. 54, No. 1, pp. 109–133. https://doi.org/10.1016/S0143-974X(99)00051-6

Ojalvo, M. (2011), "Opposing Theories and the Buckling Strength of Unequal-Leg Angle Columns," *Journal of Structural Engineering,* Vol. 137, No. 10, pp. 1104–1106. https://doi.org/10.1061/(ASCE)ST.1943-541X.0000389

Olsson, A. (2001), "Stainless Steel Plasticity: Material Modelling and Structural Applications," Doctoral Dissertation, Luleå University of Technology, Luleå, Sweden.

Quach, W., Teng, J.G., and Chung, K.F. (2008), "Three-Stage Full-Range Stress-Strain Model for Stainless Steels," *Journal of Structural Engineering,* Vol. 134, No. 9, pp. 1518–1527. https://doi.org/10.1061/(ASCE)0733-9445(2008)134:9(1518)

Rasmussen, K.J. (2003), "Full-Range Stress–Strain Curves for Stainless Steel Alloys," *Journal of Constructional Steel Research,* Vol. 59, No. 1, pp. 47–61. https://doi.org/10.1016/S0143-974X(02)00018-4

Rasmussen, K.J. (2005), "Design of Angle Columns with Locally Unstable Legs," *Journal of Structural Engineering,* Vol. 131, No. 10, pp. 1553–1560. https://doi.org/10.1061/(ASCE)0733-9445(2005)131:10(1553)

Reynolds, N.A. (2013), "Behavior and Design of Concentrically Loaded Duplex Stainless Steel Single Equal-Leg Angle Struts," Doctoral Dissertation, Georgia Institute of Technology, Atlanta, Ga.

Sarquis, F.R., Lima, L.R.O. de, da S. Vellasco, P.C.G., and Rodrigues, M.C. (2020), "Experimental and Numerical Investigation of Hot-Rolled Stainless Steel Equal Leg Angles under Compression," *Thin-Walled Structures,* Vol. 151, 106742. https://doi.org/10.1016/j.tws.2020.106742

Schafer, B.W., Li, Z., and Moen, C.D. (2010), "Computational Modeling of Cold-Formed Steel," *Thin-Walled Structures,* Vol. 48, No. 10-11, pp. 752–762. https://doi.org/10.1016/j.tws.2010.04.008

Sippel, E.J. (2022), "Structural Analysis with Non-Symmetric Cross Sections," Doctoral Dissertation, University of Wisconsin–Madison. https://asset.library.wisc.edu/1711.dl/IAZMR5L7NRQME8F/R/file-e9e51.pdf

Sirqueira, A.d.S., Vellasco, P.C.S., Lima, L.R.O. de, and Sarquis, F.R. (2020), "Experimental Assessment of Stainless Steel Hot-Rolled Equal Legs Angles in Compression," *Journal of Constructional Steel Research,* Vol. 169, 106069. https://doi.org/10.1016/j.jcsr.2020.106069

Sun, Y., Liu, Z., Liang, Y., and Zhao, O. (2019), "Experimental and Numerical Investigations of Hot-Rolled Austenitic Stainless Steel Equal-Leg Angle Sections," *Thin-Walled Structures,* Vol. 144, 106225. https://doi.org/10.1016/j.tws.2019.106225

Timoshenko, S. and Gere, J. (1961), *Theory of Elastic Stability*, 2nd Ed., McGraw-Hill Book Company, New York, N.Y.

Wu, F.-H. (1982), "Experimental Determination of Buckling Loads for Unequal Leg Angles with Concentric Loads," Master's Thesis, Ohio State University, Columbus, Ohio.

Zhang, L., Liang, Y., and Zhao, O. (2020), "Experimental and Numerical Investigations of Pin-Ended Hot-Rolled Stainless Steel Angle Section Columns Failing by Flexural Buckling," *Thin-Walled Structures,* Vol. 156, 106977. https://doi.org/10.1016/j.tws.2020.106977

Zhang, L., Liang, Y., and Zhao, O. (2021), "Laboratory Testing and Numerical Modelling of Pin-Ended Hot-Rolled Stainless Steel Angle Section Columns Failing by Flexural-Torsional Buckling," *Thin-Walled Structures,* Vol. 161, 107395. https://doi.org/10.1016/j.tws.2020.107395

Zhang, L., Tan, K.H., and Zhao, O. (2019), "Experimental and Numerical Studies of Fixed-Ended Cold-Formed Stainless Steel Equal-Leg Angle Section Columns," *Engineering Structures,* Vol. 184, pp. 134–144. https://doi.org/10.1016/j.engstruct.2019.01.083

Zhang, Y., Bu, Y., Wang, Y., Wang, Z., and Ouyang, Y. (2021), "Study of Flexural–Torsional Buckling Behaviour of 6061-T6 Aluminium Alloy Unequal-Leg Angle Columns," *Thin-Walled Structures,* Vol. 164, 107821. https://doi.org/10.1016/j.tws.2021.107821

Zhang, Y., Wang, Y., Wang, Z., Bu, Y., Fan, S., and Zheng, B. (2020), "Experimental Investigation and Numerical Analysis of Pin-Ended Extruded Aluminium Alloy Unequal Angle Columns," *Engineering Structures,* Vol. 215, 110694. https://doi.org/10.1016/j.engstruct.2020.110694

Ziemian, R.D. (2010), *Guide to Stability Design Criteria for Metal Structures*, 6th Ed., John Wiley & Sons, Hoboken, N.J.